

## FADTTS: Functional analysis of diffusion tensor tract statistics<sup>☆</sup>

Hongtu Zhu<sup>a,e,\*</sup>, Linglong Kong<sup>a</sup>, Runze Li<sup>f</sup>, Martin Styner<sup>b,c</sup>, Guido Gerig<sup>g</sup>, Weili Lin<sup>d,e</sup>, John H. Gilmore<sup>c</sup>

<sup>a</sup> Department of Biostatistics, University of North Carolina at Chapel Hill, Chapel Hill, NC 27599, USA

<sup>b</sup> Department of Computer Science, University of North Carolina at Chapel Hill, Chapel Hill, NC 27599, USA

<sup>c</sup> Department of Psychiatry, University of North Carolina at Chapel Hill, Chapel Hill, NC 27599, USA

<sup>d</sup> Department of Radiology, University of North Carolina at Chapel Hill, Chapel Hill, NC 27599, USA

<sup>e</sup> Biomedical Research Imaging Center, University of North Carolina at Chapel Hill, Chapel Hill, NC 27599, USA

<sup>f</sup> Department of Statistics and The Methodology Center, The Pennsylvania State University, University Park, PA 16802, USA

<sup>g</sup> Scientific Computing and Imaging Institute, The University of Utah, Salt Lake City, UT 84100, USA

### ARTICLE INFO

#### Article history:

Received 7 October 2010

Revised 19 January 2011

Accepted 28 January 2011

Available online 16 February 2011

#### Keywords:

Confidence band

Diffusion tensor imaging

Fiber bundle

Global test statistic

Varying coefficient model

### ABSTRACT

The aim of this paper is to present a functional analysis of a diffusion tensor tract statistics (FADTTS) pipeline for delineating the association between multiple diffusion properties along major white matter fiber bundles with a set of covariates of interest, such as age, diagnostic status and gender, and the structure of the variability of these white matter tract properties in various diffusion tensor imaging studies. The FADTTS integrates five statistical tools: (i) a multivariate varying coefficient model for allowing the varying coefficient functions in terms of arc length to characterize the varying associations between fiber bundle diffusion properties and a set of covariates, (ii) a weighted least squares estimation of the varying coefficient functions, (iii) a functional principal component analysis to delineate the structure of the variability in fiber bundle diffusion properties, (iv) a global test statistic to test hypotheses of interest, and (v) a simultaneous confidence band to quantify the uncertainty in the estimated coefficient functions. Simulated data are used to evaluate the finite sample performance of FADTTS. We apply FADTTS to investigate the development of white matter diffusivities along the splenium of the corpus callosum tract and the right internal capsule tract in a clinical study of neurodevelopment. FADTTS can be used to facilitate the understanding of normal brain development, the neural bases of neuropsychiatric disorders, and the joint effects of environmental and genetic factors on white matter fiber bundles. The advantages of FADTTS compared with the other existing approaches are that they are capable of modeling the structured inter-subject variability, testing the joint effects, and constructing their simultaneous confidence bands. However, FADTTS is not crucial for estimation and reduces to the functional analysis method for the single measure.

© 2011 Elsevier Inc. All rights reserved.

### Introduction

Diffusion tensor imaging (DTI), which can track the effective diffusion of water in the human brain in vivo, has been widely used to map the structure and orientation of the white matter fiber tracts of the brain (Basser et al., 1994a,b). In DTI, the degree of diffusivity and the directional dependence of water diffusion in each voxel can be

quantified by a  $3 \times 3$  matrix, called a diffusion tensor (DT), and its tensor-derived quantities. These quantities are called diffusion properties. They include the three eigenvalue–eigenvector pairs of DT and other related parameters, such as fractional anisotropy (FA) (Pierpaoli and Basser, 1996; Hasan et al., 2001; Hasan and Narayana, 2003; Zhu et al., 2006). A wealth of neuroimaging studies have been conducted to use these tensor-derived quantities as a marker for white matter tract maturation and integrity in order to better understand normal brain development and the neural bases of neuropsychiatric and neuro-degenerative disorders (Moseley, 2002; Mukherjee and McKinstry, 2006; Cascio et al., 2007; Rollins, 2007).

In the current literature, there are three major approaches to the group analysis of diffusion imaging data: region-of-interest (ROI) analysis, voxel based analysis, and fiber tract based analysis (Smith et al., 2006; O'Donnell et al., 2009; Snook et al., 2007). The ROI analysis used in some neuroimaging studies (Bonekam et al., 2008; Gilmore et al., 2008) primarily averages diffusion properties in some manually drawn ROIs for each subject and then creates a single statistic per ROI (Snook et al., 2007). The main drawbacks of ROI analysis are the

<sup>☆</sup> This work was supported in part by NSF grant BCS-08-26844 and NIH grants RR025747-01, P01CA142538-01, MH086633, and AG033387 to Dr. Zhu, NSF grant DMS 0348869, NIH grants P50-DA10075 and R21-DA024260 and NNSF of China 11028103 to Dr. Li, NIH grants MH064065, HD053000, and MH070890 to Dr. Gilmore, NIH grants R01NS055754 and R01EB5-34816 to Dr. Lin, Lilly Research Laboratories, the UNC NDRC HD 03110, Eli Lilly grant F1D-MC-X252, and NIH Roadmap Grant U54 EB005149-01, NAMIC to Dr. Styner. The content is solely the responsibility of the authors and does not necessarily represent the official views of the NSF or the NIH. The readers are welcome to request reprints from Dr. Hongtu Zhu.

\* Corresponding author at: Department of Biostatistics, University of North Carolina at Chapel Hill, Chapel Hill, NC 27599, USA.

E-mail address: [htzhu@email.unc.edu](mailto:htzhu@email.unc.edu) (H. Zhu).

difficulty in identifying meaningful ROIs, particularly the long curved structures common in fiber tracts; the instability of statistical results obtained from ROI analysis, and the partial volume effect in relatively large ROIs (Goodlett et al., 2009; Zhu et al., 2010c). A stringent assumption of the ROI analysis is that diffusion properties in all voxels of the same ROI are essentially homogeneous, which is largely false for DTI.

Voxel-based analysis is used more commonly than ROI analysis in neuroimaging studies (Chen et al., 2009; Focke et al., 2008; Camara et al., 2007; Snook et al., 2005). It usually involves fitting a statistical model to the smoothed and registered diffusion property imaging data from multiple subjects at each voxel to generate a parametric map of test statistics (or  $p$ -values). Subsequently, a multiple comparisons procedure such as random field theory is applied to correct for multiple comparisons across the many voxels of the imaging volume (Ashburner and Friston, 2000; Wager et al., 2005; Worsley et al., 2004). The major drawbacks of voxel based analysis include poor alignment quality and the arbitrary choice of smoothing extent (Hecke et al., 2009; Ashburner and Friston, 2000; Smith et al., 2006; Jones et al., 2005). Particularly, extensive simulation results have shown that the final results of voxel-based analysis can strongly depend on the amount of smoothing in the smoothed diffusion imaging data (Jones et al., 2005).

With the drawbacks of the ROI and voxel based analyses, there is a growing interest in the DTI literature on developing fiber tract based analysis of diffusion properties (Smith et al., 2006; O'Donnell et al., 2009; Yushkevich et al., 2008; Goodlett et al., 2009; Zhu et al., 2010c). For instance, a *tract-based spatial statistics* framework was developed to construct local diffusion properties along the white matter skeleton and then perform pointwise hypothesis tests on the skeleton (Smith et al., 2006). A model-based framework was developed for statistically analyzing diffusion properties on the medial manifolds of fiber tract followed by testing pointwise hypotheses on the medial manifolds (Yushkevich et al., 2008). These two methods essentially ignore the functional nature of diffusion properties in terms of arc length along the white matter skeleton and the medial manifolds, and thus they suffer from low statistical power in detecting interesting features and exploring variability in functional data. Statistically, diffusion properties along fiber bundles are functional data of position along the tract. Formal analysis of these fiber bundle diffusion properties requires recently developed advanced functional data analysis methods (Li and Hsing, 2010; Yao and Lee, 2006; Hall et al., 2006; Ramsay and Silverman, 2005, 2002).

There are several developments on the use of functional data analysis methods for the statistical analysis of diffusion properties along fiber tracts. Goodlett and his coauthors used the functional principal component analysis coupled with the Hotelling  $T^2$  statistic to compare a univariate diffusion property, such as fractional anisotropy, across two (or more) populations for a single hypothesis test per tract (Goodlett et al., 2009; Ramsay and Silverman, 2005). Their method is “smoothing first, then estimation.” This method is limited to a univariate diffusion property and cannot control for other continuous covariates of interest, such as age. The constraint principal component analysis method was used by Gouttard and his coauthors to fit the age related changes of diffusion properties along fiber tracts (Gouttard et al., 2009). Three major limitations of their method are that it only fits a univariate diffusion property; it cannot control for multiple covariates of interest, such as age and gender; and it cannot test a hypothesis of interest, such as age effect. Zhu and his coauthors presented a functional regression analysis of DTI tract statistics, called FRATS, for the analysis of multiple diffusion properties along fiber bundles with a set of covariates of interest (Zhu et al., 2010c). FRATS is also “smoothing first, then estimation,” and is executed in two steps (Zhu et al., 2010c; Zhang and Chen, 2007). The first step is to smooth multiple diffusion properties along individual fiber bundles using the local polynomial kernel method. The second step is to fit a functional linear model with varying coefficient functions to directly characterize the association between the smoothed fiber bundle diffusion properties and a set of covariates, and then to test the hypothesis of

interest. However, their method does not include methods for delineating the structure of the variability in fiber bundle diffusion properties or for quantifying the uncertainty in the estimated coefficient functions. Zhu and his coauthors developed a multivariate varying coefficient model, but their statistical methods only include estimation methods and statistics for testing hypothesis of interest (Zhu et al., 2010a). Greven and her coauthors also developed a univariate varying coefficient model for longitudinal functional data, but they have not developed any formal statistics for testing hypotheses and constructing the confidence band of any varying coefficient function in a frequentist framework (Greven et al., 2010).

This paper will present a functional analysis of the diffusion tensor tract statistics (FADTTS) pipeline for delineating the structure of the variability of multiple diffusion properties along major white matter fiber bundles and their association with a set of covariates. Diffusion properties, such as fractional anisotropy (FA) and mean diffusivity (MD), along fiber tracts are modeled as functions of the position along the tracts. Compared with the existing literature (Goodlett et al., 2009; Zhu et al., 2010c, 2010a; Greven et al., 2010), there are five methodological contributions in this paper. First, a multivariate varying coefficient model is developed to characterize the association between fiber bundle diffusion properties and a set of covariates. Second, a weighted least squares estimation is proposed to directly estimate the varying coefficient functions without using the “smoothing first, then estimation” strategy. Third, a functional principal component analysis is employed to delineate the structure of the variability in fiber bundle diffusion properties. Fourth, under the multivariate varying coefficient model, a global test statistic is proposed to test hypotheses of interest and a resampling method is developed for approximating the  $p$ -value of the global test statistic. Fifth, a simultaneous confidence band is built to quantify the uncertainty in the estimated coefficient functions and a resampling method is proposed to approximate the critical point. The advantages of FADTTS are that they are capable of modeling the structured inter-subject variability by a functional principal component analysis method, testing the joint effects by a global test statistic and local test statistics, and constructing simultaneous confidence bands of the interested effects through a resampling method. However, FADTTS is not crucial for estimation and reduces to the functional analysis method for the single measure (Zellner, 1962).

## Methodologies

The focus of this paper is to present a functional analysis pipeline, called FADTTS, with five powerful statistical tools for delineating the structure of the variability of multiple diffusion properties along major white matter fiber bundles and their association with a set of covariates of interest, such as age. Mathematically, we have rigorously derived the asymptotic properties of FADTTS, whose detailed assumptions and proofs are available from the first author upon request (Zhu et al., 2010b). A schematic overview of FADTTS is given in Fig. 1. The code for FADTTS was written in Matlab, which along with its documentation is freely accessible from our website “<http://www.nitrc.org/projects/fadtts>”. To make it easily accessible, we developed a Graphical User Interface (GUI) to pack the code, also freely downloadable from the same website.

To compare diffusion properties in populations of DTIs, we use DTI atlas building followed by atlas fiber tractography and fiber parametrization as described in Goodlett et al. (2009) to extract DTI fibers and establish DTI fiber correspondence across all DTI datasets from different subjects. Since this method has been described in detail (Goodlett et al., 2009; Zhu et al., 2010c), we do not include a description here for the sake of simplicity. We briefly describe each component of FADTTS in the following subsections, and their technical details can be found in Zhu et al. (2010b).

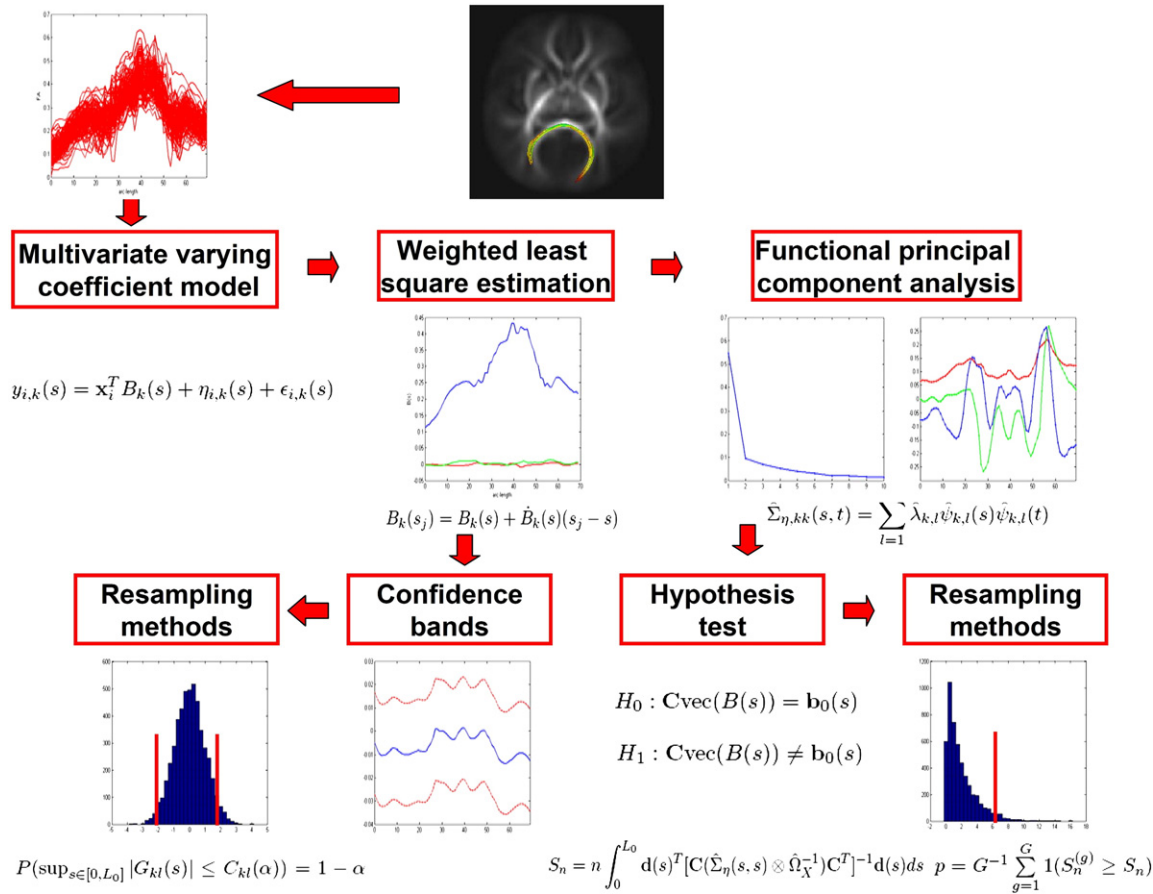


**Fig. 1.** A schematic overview of FADTTS: a multivariate varying coefficient model for the diffusion properties of a tract, a weighted least squares method for estimating the coefficient functions, a functional principal component analysis model for analyzing the covariance structure, a hypothesis test for coefficient functions using both local and global test statistics, a resampling method for estimating the  $p$ -value of the global test statistics, and a method for constructing the confidence bands of the coefficient functions based on a resampling method.

### Multivariate varying coefficient model

We develop a *multivariate varying coefficient model* to model  $J$  diffusion quantities (e.g., FA) measured along fiber bundles with a set of covariates of interest. The  $J$  diffusion properties along fiber tracts are treated as functional data, which are functions of the position of the tracts and have no connection with functional magnetic resonance imaging data. Let  $s \in [0, L]$  be the arc length of any point on a specific fiber bundle relative to a fixed end point of the fiber bundle, where  $L$  is the longest arc length on the fiber bundle. For the  $i$ -th subject, we consider a  $J \times 1$  vector of diffusion properties, denoted by  $\mathbf{y}_i(s_m) = (y_{i,1}(s_m), \dots, y_{i,J}(s_m))^T$ , and its associated arc length  $s_m$  for the  $m$ -th location grid point on the fiber bundle for  $i = 1, \dots, n$  and  $m = 1, \dots, M$ , where  $n$  and  $M$  denote the numbers of subjects and grid points, respectively. We consider a multivariate varying coefficient model (Fan and Zhang, 1999; Wu and Chiang, 2000; Fan et al., 2003; Fan and Zhang, 2008; Wang et al., 2008; Ferguson et al., 2009), which assumes that for  $i = 1, \dots, n$  and  $j = 1, \dots, J$ ,

$$y_{i,j}(s) = \mathbf{x}_i^T B_j(s) + \eta_{i,j}(s) + \epsilon_{i,j}(s), \quad (1)$$

where  $B_j(s) = (\beta_{j1}(s), \dots, \beta_{jp}(s))^T$  is a  $p \times 1$  vector of coefficient functions of arc length  $s$ ,  $\mathbf{x}_i$  is a  $p \times 1$  vector of covariates of interest with  $x_{i,1} = 1$ , and  $\epsilon_{i,j}(s)$  are measurement errors. Moreover,  $\eta_{i,j}(s)$  characterizes both individual curve variations from  $\mathbf{x}_i^T B_j(s)$  and the correlation between  $y_{i,j}(s)$  and  $y_{i,j}(t)$  for different  $s$  and  $t$ . That is,  $\eta_{i,j}(s)$  measures both subject-specific variability and location-specific variability. In addition,  $\beta_{j1}(s)$  describes the average curve (i.e., the typical curve), of the  $j$ -th diffusion property.

It is also assumed that  $\eta_i(s) = (\eta_{i,1}(s), \dots, \eta_{i,J}(s))^T$  and  $\epsilon_i(s) = (\epsilon_{i,1}(s), \dots, \epsilon_{i,J}(s))^T$  are mutually independent, and  $\eta_i(s)$  and  $\epsilon_i(s)$  are, respectively, independent and identical copies of  $SP(0, \Sigma_{\eta})$  and  $SP(0, \Sigma_{\epsilon})$ , where  $SP(\mu, \Sigma)$  denotes a vector with elements being stochastic processes with mean function  $\mu(s)$  and covariance function  $\Sigma(s, t)$  for any  $s, t \in [0, L]$ . Moreover, for any  $1 \leq u, v \leq M$ , the covariance structure of  $\mathbf{y}_i(s)$ , denoted by  $\Sigma_{\mathbf{y}}(s, t) = (\Sigma_{y,uv}(s, t))$ , is given by

$$\Sigma_{y,uv}(s, t) = \text{Cov}(\mathbf{y}_{i,u}(s), \mathbf{y}_{i,v}(t)) = \Sigma_{\eta,uv}(s, t) + \Sigma_{\epsilon,uv}(s, t)1(s = t), \quad (2)$$

where  $\Sigma_{\eta,uv}(s, t)$  and  $\Sigma_{\epsilon,uv}(s, t)$  are the  $(u, v)$ -th component of  $M \times M$  matrices  $\Sigma_{\eta}(s, t)$  and  $\Sigma_{\epsilon}(s, t)$ , respectively.

Since the design matrix is the same for all diffusion properties, the estimators of  $B_j(s)$  for  $j = 1, 2, \dots, J$  from Eq. (1) obtained by pooling all diffusion properties together are identical to those obtained by fitting diffusion properties individually (Zellner, 1962). However, the covariance structure of  $\mathbf{y}_i(s)$  plays an essential role in the inference procedure (e.g. hypothesis test and confidence bands), which can only be estimated by pooling all diffusion properties together using model (1). Moreover, in practice, it is also interesting to compare different tensor-derived statistics along the tract, and thus a functional analysis method for multiple outcomes is necessary and useful. For instance, in real data analysis, one may be interested in testing which eigenvalue grows faster (Zhu et al., 2010c).

As an illustration, in our clinical study on early brain development, we are interested in studying the evolution of the three eigenvalues  $\lambda_j$ ,  $j = 1, 2, 3$ , of diffusion tensor ( $\lambda_1 \geq \lambda_2 \geq \lambda_3$ ) along two selected fiber tracts in 128 healthy pediatric subjects (Figs. 4(a) and 8(a)). We

consider a multivariate varying coefficient model of three eigenvalues along a specific tract as follows:

$$\begin{aligned} L_{i,1}(s) &= \beta_{11}(s) + \beta_{12}(s) \times G_i + \beta_{13}(s) \times \text{Gage}_i + \eta_{i,1}(s) + \epsilon_{i,1}(s), \\ L_{i,2}(s) &= \beta_{21}(s) + \beta_{22}(s) \times G_i + \beta_{23}(s) \times \text{Gage}_i + \eta_{i,2}(s) + \epsilon_{i,2}(s), \quad (3) \\ L_{i,3}(s) &= \beta_{31}(s) + \beta_{32}(s) \times G_i + \beta_{33}(s) \times \text{Gage}_i + \eta_{i,3}(s) + \epsilon_{i,3}(s), \end{aligned}$$

where  $L_{i,j}(s)$  equals  $L_j$  at the location  $s$  for  $j = 1, 2, 3$  and  $i = 1, \dots, 128$  and  $G_i$  and  $\text{Gage}_i$ , respectively, denote the gender and the gestational age at the scan time of the  $i$ -th infant. In this case,  $J = 3$ ,  $B_j(s) = (\beta_{j1}(s), \beta_{j2}(s), \beta_{j3}(s))^T$ , and  $\mathbf{x}_i = (1, G_i, \text{Gage}_i)^T$ .

*Weighted least squares estimation*

To estimate the coefficient functions in  $\mathbf{B}(s) = [B_1(s), B_2(s), \dots, B_j(s)]$ , we employ a weighted least squares (WLS) method based on a local polynomial kernel (LPK) smoothing technique (Fan and Gijbels, 1996; Wand and Jones, 1995; Wu and Zhang, 2006; Ramsay and Silverman, 2005; Welsh and Yee, 2006; Zhang and Chen, 2007). Specifically, using Taylor's expansion, we can expand  $B_j(s_m)$  at  $s$  to obtain

$$B_j(s_m) = B_j(s) + \dot{B}_j(s)(s_m - s), \quad (4)$$

where  $\dot{B}_j(s) = (\dot{\beta}_{j1}(s), \dots, \dot{\beta}_{jp}(s))^T$  and  $\dot{\beta}_{jl}(s) = d\beta_{jl}(s) / ds$  for  $l = 1, \dots, p$ . Let  $K(\cdot)$  be a kernel function, such as the Gaussian and uniform kernels (Fan and Gijbels, 1996; Wand and Jones, 1995). For a fixed bandwidth  $h$  and each  $j$ , the WLS estimator of  $B_j(s)$  is obtained by minimizing an objective function

$$\sum_{i=1}^n \sum_{m=1}^M \left[ y_{ij}(s_m) - \mathbf{x}_i^T A_j(h, s_m - s) \mathbf{z}(h, s_m - s) \right]^2 K((s_m - s) / h) / h, \quad (5)$$

where  $A_j(h, s_m - s) = [B_j(s), h\dot{B}_j(s)(s_m - s)]$  and  $\mathbf{z}(h, s_m - s) = (1, (s_m - s) / h)^T$ . The WLS method differs from the standard least squares method by only incorporating observations measured at those grid points near each point  $s$ .

To select an optimal bandwidth, we use the leave-one-out generalized cross-validation score method for simplicity and computational efficiency (Zhang and Chen, 2007; Zhu et al., 2010b). Other bandwidth selection methods, such as Bayesian evidence optimization, can be implemented directly as well. In practice, we standardize all covariates and diffusion properties to have mean zero and standard deviation one and then choose a common bandwidth for all covariates. This greatly increases computational efficiency in bandwidth selection. Moreover, the estimation results are fairly robust to the bandwidth selection unless an extremely small or large bandwidth is chosen. Based on our experience in simulation studies, we recommend searching around  $\max\{30, M/2\}$  log-spaced points from  $1/M$  to  $1/8$  of the arc length range. For each diffusion property, we select an optimal bandwidth and compute the corresponding estimator of  $B_j(s)$ , denoted by  $\hat{B}_j(s)$ , at the optimal bandwidth.

*Functional principal component analysis*

To simultaneously construct all individual functions  $\eta_{i,j}(s)$ , we also employ the PLK smoothing technique (Fan and Gijbels, 1996; Wand and Jones, 1995; Wu and Zhang, 2006; Ramsay and Silverman, 2005; Welsh and Yee, 2006; Zhang and Chen, 2007). Specifically, using Taylor's expansion, we can expand  $\eta_{i,j}(s_m)$  at  $s$  to obtain  $\eta_{i,j}(s_m) = \eta_{i,j}(s) + \dot{\eta}_{i,j}(s)(s_m - s)$ . We develop an algorithm based on

WLS with LPK to estimate  $\eta_{i,j}(s)$  as follows. For each  $j$  and a fixed bandwidth  $h$ , we estimate  $\eta_{i,j}(s)$  by minimizing an objective function

$$\sum_{m=1}^M \left[ y_{ij}(s_m) - \mathbf{x}_i^T \hat{B}_j(s_m) - D_{ij}(h, s_m - s) \mathbf{z}(h, s_m - s) \right]^2 K((s_m - s) / h) / h, \quad (6)$$

where  $D_{ij}(h, s_m - s) = [\eta_{i,j}(s), h \dot{\eta}_{i,j}(s)(s_m - s)]$ .

Pooling all the data from  $n$  subjects for each  $j$ , the optimal bandwidth is selected by using the leave-one-out generalized cross-validation score method. Based on the optimal bandwidth, we can estimate  $\eta_{i,j}(s)$  and  $\eta_i(s)$ , denoted by  $\hat{\eta}_{i,j}(s)$  and  $\hat{\eta}_i(s)$ , respectively, for all  $i$  and  $j$ . We then use their empirical mean and covariance to estimate  $\eta(s)$  and  $\Sigma_\eta(s, t)$ . The estimator of  $\Sigma_\eta(s, t)$  is a weighted mean of the empirical covariances of  $\hat{\epsilon}_i(s_m) = \mathbf{y}_i(s_m) - \hat{\mathbf{B}}(s_m)^T \mathbf{x}_i - \hat{\eta}_i(s_m)$  by a kernel approach with the optimal bandwidth selected by the cross validation method.

Functional principal component analysis (FPCA) attempts to find the dominant modes of variation around regression functions, and is thus a key technique in functional data analysis (Li and Hsing, 2010; Yao and Lee, 2006; Hall et al., 2006; Ramsay and Silverman, 2005; Ramsay and Silverman, 2002). We calculate the spectral decomposition of  $\hat{\Sigma}_{\eta_{ij}}(s, t)$  for each  $j$  as follows:

$$\hat{\Sigma}_{\eta_{ij}}(s, t) = \sum_{l=1}^{\infty} \hat{\lambda}_{j,l} \hat{\psi}_{j,l}(s) \hat{\psi}_{j,l}(t), \quad (7)$$

where  $\hat{\lambda}_{j,1} \geq \hat{\lambda}_{j,2} \geq \dots \geq 0$  are estimated eigenvalues and the  $\hat{\psi}_{j,l}(t)$ 's are the corresponding estimated principal components. For finite  $M$ , we essentially have the regular principal component analysis (PCA). That is, we have a finite number of estimated non-zero eigenvalues, which are the eigenvalues of  $(\hat{\Sigma}_{\eta_{ij}}(s_u, s_v))$  for  $u, v = 1, \dots, M$ , and the estimated principal components  $[\hat{\psi}_{j,l}(s_1), \dots, \hat{\psi}_{j,l}(s_M)]$  are the  $l$ -th eigenfunction of  $(\hat{\Sigma}_{\eta_{ij}}(s_u, s_v))$ . In practice, we use the proportion of variance explained greater than 80% to truncate eigenvalues.

*Hypothesis test*

In neuroimaging studies, most scientific questions require the comparison of fiber bundle diffusion properties along fiber bundles across two (or more) diagnostic groups and the assessment of the development of fiber bundle diffusion properties across age. Such questions can often be formulated as linear hypotheses of  $B(s)$  as follows:

$$H_0 : \mathbf{C} \text{vec}(B(s)) = \mathbf{b}_0(s) \text{ for all } s \text{ vs. } H_1 : \mathbf{C} \text{vec}(B(s)) \neq \mathbf{b}_0(s), \quad (8)$$

where  $\mathbf{C}$  is a  $r \times Jp$  matrix of full row rank and  $\mathbf{b}_0(s)$  is a given  $r \times 1$  vector of functions.

As an illustration, in model (3), we are interested in comparing the evolution speeds of the three eigenvalues of the DTs along selected fiber tracts in 128 healthy pediatric subjects in our clinical study on early brain development. Statistically, for model (3), the comparison can be formulated as follows:

$$\begin{aligned} H_0 &: \beta_{13}(s) = \beta_{23}(s) = \beta_{33}(s) \text{ for all } s \text{ vs.} \\ H_1 &: |\beta_{13}(s) - \beta_{23}(s)| + |\beta_{23}(s) - \beta_{33}(s)| \neq 0. \end{aligned}$$

In this case, we have

$$\mathbf{C} = \begin{pmatrix} 0 & 0 & 1 & 0 & 0 & 0 & 0 & 0 & -1 \\ 0 & 0 & 0 & 0 & 0 & 1 & 0 & 0 & -1 \end{pmatrix} \text{ and } \mathbf{b}_0(s) \equiv \begin{pmatrix} 0 \\ 0 \end{pmatrix} \text{ for all } s.$$

The use of multiple diffusion properties in model (3) allows us to compare different functions in  $B(s)$  associated with different diffusion properties.

We propose both local and global test statistics. The local test statistic can identify the exact location of a significant grid point on a specific tract. At a given grid point  $s_m$  on a specific tract, we test the local null hypothesis  $H_0(s_m) : \mathbf{C} \text{vec}(B(s_m)) = \mathbf{b}_0(s_m)$  against  $H_1(s_m) : \mathbf{C} \text{vec}(B(s_m)) \neq \mathbf{b}_0(s_m)$ . The local test statistic  $S_n(s_m)$  is defined by

$$S_n(s_m) = \mathbf{d}(s_m)^T \left[ \mathbf{C} \left( \hat{\Sigma}_\eta(s_m, s_m) \otimes \hat{\Omega}_X^{-1} \right) \mathbf{C}^T \right]^{-1} \mathbf{d}(s_m), \tag{9}$$

where  $\hat{\Omega}_X^{-1} \sum_{i=1}^n \mathbf{x}_i \otimes \mathbf{x}_i^T$ ,  $\mathbf{d}(s) = \mathbf{C} \text{vec}(\hat{B}(s) - \text{bias}(\hat{B}(s))) - \mathbf{b}_0(s)$  and  $\otimes$  denote the Kronecker product. Following Fan and Zhang (2000), a smaller bandwidth leads to a small value of bias( $\hat{B}(s)$ ); thus, we drop bias( $\hat{B}(s)$ ) from now on. We test the null hypothesis  $H_0 : \mathbf{C} \text{vec}(B(s)) = \mathbf{b}_0(s)$  for all  $s$  using a global test statistic  $S_n$  defined by

$$S_n = \int_0^{L_0} \mathbf{d}(s)^T \left[ \mathbf{C} \left( \hat{\Sigma}_\eta(s, s) \otimes \hat{\Omega}_X^{-1} \right) \mathbf{C}^T \right]^{-1} \mathbf{d}(s) ds. \tag{10}$$

In order to use  $S_n$  as a test statistic, we have already shown that  $S_n$  has a desirable asymptotic distribution, a weighted  $\chi^2$  distribution. To efficiently approximate the  $p$ -value of  $S_n$ , we use a wild bootstrap method from Zhu et al. (2010b).

*Confidence bands*

For a given significance level  $\alpha$ , we construct a simultaneous confidence band for each  $\beta_{jl}(s)$  such that

$$P \left( \hat{\beta}_{jl}^{L,\alpha}(s) < \beta_{jl}(s) < \hat{\beta}_{jl}^{U,\alpha}(s) \text{ for all } s \in [0, L] \right) = 1 - \alpha, \tag{11}$$

where  $\hat{\beta}_{jl}^{L,\alpha}(s)$  and  $\hat{\beta}_{jl}^{U,\alpha}(s)$  are the lower and upper limits of the confidence band. Since  $\sup_{s \in [0, L]} |\sqrt{n} [\hat{\beta}_{jl}(s) - \beta_{jl}(s)]|$  converges in distribution to  $\sup_{s \in [0, L]} |G_{jl}(s)|$ , where  $G_{jl}(\cdot)$  is a centered Gaussian process, we define the critical point  $C_{jl}(\alpha)$  such that  $P(\sup_{s \in [0, L]} |G_{jl}(s)| \leq C_{jl}(\alpha)) = 1 - \alpha$ . Therefore, a  $1 - \alpha$  simultaneous confidence band for  $\beta_{jl}(s)$  is given as follows:

$$\left( \hat{\beta}_{jl}(s) - \frac{C_{jl}(\alpha)}{\sqrt{n}}, \hat{\beta}_{jl}(s) + \frac{C_{jl}(\alpha)}{\sqrt{n}} \right). \tag{12}$$

We develop an efficient resampling method to approximate  $C_{jl}(\alpha)$  as in Zhu et al. (2007a) and Kosorok (2003).

**Simulation studies and a real example**

We will use two sets of Monte Carlo simulations and a real example to evaluate the finite-sample performance of FADTTS. All computations for these numerical examples were done in matlab on an IBM ThinkCentre M50 workstation. The computation time for FADTTS is relatively efficient. For example, for our real example with  $n = 128, J = 5, M = 75$  and  $p = 3$ , the FADTTS procedure including 500 wild bootstrap samples took an average CPU time of about 13 min. The computational time for FADTTS can be further reduced by using other computer languages, such as C++.

*Simulation studies*

We conducted two sets of Monte Carlo simulations to evaluate the Types I and II error rates of the global test statistic  $S_n$  and the coverage probabilities of the simultaneous confidence bands of the functional coefficients  $B(s)$ , respectively. In the first set of simulations, we evaluated the Types I and II error rates by simulating FA and MD measures (Figs. 8(b) and (c)) along the right internal capsule tract according to

$$(\text{FA}_i(s_m), \text{MD}_i(s_m))^T = (\mathbf{x}_i^T B_1(s_m), \mathbf{x}_i^T B_2(s_m))^T + \eta_i(s_m) + \epsilon_i(s_m),$$

$$\begin{aligned} \mathbf{x}_i^T B_1(s) &= \beta_{11}(s) + \beta_{12}(s) \times G_i + \beta_{13}(s) \times \text{Gage}_i, \\ \mathbf{x}_i^T B_2(s) &= \beta_{21}(s) + \beta_{22}(s) \times G_i + \beta_{23}(s) \times \text{Gage}_i, \end{aligned} \tag{13}$$

where  $G_i$  and  $\text{Gage}_i$ , respectively, denote gender and the gestational age at the scan time of the  $i$ -th infant;  $\eta_i(s) = (\eta_{i1}(s), \eta_{i2}(s))^T$  is a Gaussian process with zero mean and covariance matrix  $\Sigma_\eta(s, t)$ ; and  $\epsilon_i(s) = (\epsilon_{i1}(s), \epsilon_{i2}(s))^T$  is a Gaussian random vector with zero mean and covariance matrix  $\Sigma_\epsilon(s, t)1(s=t)$ . We used the FA and MD measures along the right internal capsule tract from all the 128 infants in our clinical data to estimate  $\hat{B}(s)$  of  $B(s)$ ,  $\hat{\eta}(s)$  of  $\eta(s)$ , and  $\hat{\epsilon}(s)$  of  $\epsilon(s)$  via  $\hat{\epsilon}(s) = (\text{FA}(s), \text{MD}(s))^T - \hat{B}(s)^T \mathbf{x} - \hat{\eta}(s)$ . We fixed all the parameters at their values obtained from our clinical data, except that we assumed  $(\beta_{13}(s), \beta_{23}(s)) = c(\hat{\beta}_{13}(s), \hat{\beta}_{23}(s))$ , where  $c$  is a scalar specified below and  $(\hat{\beta}_{13}(s), \hat{\beta}_{23}(s))$  were estimators obtained from our clinical data. To mimic imaging data, we used a simulation method as follows. We generated random samples  $\tau_i^{(g)}$  and  $\tau_i(s_m)^{(g)}$  from a  $N(0, 1)$  generator for  $i = 1, \dots, n$  and  $m = 1, \dots, M$  and then constructed

$$\begin{aligned} \text{FA}_i(s_m)^{(g)} &= \hat{\beta}_{11}(s_m) + \hat{\beta}_{12}(s_m) \times G_i + c\hat{\beta}_{13}(s_m) \times \text{Gage}_i \\ &\quad + \tau_i^{(g)} \hat{\eta}_{i1}(s_m) + \tau_i(s_m)^{(g)} \hat{\epsilon}_{i1}(s_m), \\ \text{MD}_i(s_m)^{(g)} &= \hat{\beta}_{21}(s_m) + \hat{\beta}_{22}(s_m) \times G_i + c\hat{\beta}_{23}(s_m) \times \text{Gage}_i \\ &\quad + \tau_i^{(g)} \hat{\eta}_{i2}(s_m) + \tau_i(s_m)^{(g)} \hat{\epsilon}_{i2}(s_m). \end{aligned}$$

Our tests were based on the simulated values of FA and MD measures  $\text{FA}_i(s_m)^{(g)}$  and  $\text{MD}_i(s_m)^{(g)}$  for  $i = 1, \dots, n$  and  $m = 1, \dots, M$ .

As already mentioned, in neuroimaging studies, a lot of scientific questions require assessment of the development of fiber bundle diffusion properties across age. In this simulation study, we formulated questions as the hypotheses test  $H_0 : \beta_{13}(s) = \beta_{23}(s) = 0$  for all  $s$  along the right internal capsule tract against  $H_1 : \beta_{13}(s) \neq 0$  or  $\beta_{23}(s) \neq 0$  for at least one  $s$  on the tract. We first assumed  $c = 0$  to assess the Type I error rates for the global test statistic  $S_n$ , and then we assumed  $c = 0.2, 0.4, 0.6$ , and  $0.8$  to examine the Type II error rates for  $S_n$  at different effect sizes. In both cases,

$$\mathbf{C} = \begin{pmatrix} 0 & 0 & 1 & 0 & 0 & 0 \\ 0 & 0 & 0 & 0 & 0 & 1 \end{pmatrix} \text{ and } \mathbf{b}_0(s) \equiv \begin{pmatrix} 0 \\ 0 \end{pmatrix} \text{ for all } s.$$

To evaluate the Types I and II error rates at different sample sizes, we let  $n = 128$  and  $64$ . For  $n = 128$ , the values of gender and gestational age were set the same as the 128 infants in our clinical study. For  $n = 64$ , we randomly chose 32 males and 32 females from the 128 infants and used their values for gender and gestational age to simulate the values of FA and MD along the right internal capsule tract. Note that the number of grid points on the right internal capsule equals  $M = 75$  for both cases.

We applied the FADTTS procedure to the simulated values for FA and MD. Particularly, we approximated the  $p$ -value of  $S_n$  using the wild bootstrap method. For each simulation, the significance levels were set at  $\alpha = 0.05$  and  $0.01$ , and 500 replications were used to estimate the rejection rates. For a fixed  $\alpha$ , if the Type I rejection rate is smaller than  $\alpha$ , then the test is conservative, whereas if the Type I rejection rate is greater than  $\alpha$ , then the test is anticonservative, or liberal. The Monte Carlo error rate is  $\sqrt{\alpha(1-\alpha)/N}$  with  $N = 500$ .

As shown in Table 1, the rejection rates for  $S_n$  based on the resampling method are relatively accurate for all sample sizes ( $n = 64$ , or  $128$ ) and all effect sizes ( $c = 0, 0.2, 0.4, 0.6$ , or  $0.8$ ) at both significance levels ( $\alpha = 0.01$  or  $0.05$ ) (Figs. 2(a) and (b);  $n = 64$  and Figs. 2(c) and (d);  $n = 128$ ). The statistical power for rejecting the null hypothesis increases with the sample size and the effect size, which is consistent with our expectation. In addition, to show that FADTTS

**Table 1**  
Simulation study: the Type I and Type II error rates of  $S_n$  under GLM and FADTTS.

	Sample size $n = 64$				Sample size $n = 128$			
	$\alpha = 0.01$		$\alpha = 0.05$		$\alpha = 0.01$		$\alpha = 0.05$	
	GLM	FADTTS	GLM	FADTTS	GLM	FADTTS	GLM	FADTTS
$c = 0.000$	0.000	0.005	0.040	0.045	0.005	0.005	0.045	0.060
$c = 0.200$	0.005	0.030	0.065	0.115	0.015	0.045	0.075	0.165
$c = 0.400$	0.020	0.085	0.110	0.275	0.065	0.150	0.240	0.370
$c = 0.600$	0.085	0.185	0.210	0.420	0.140	0.310	0.390	0.600
$c = 0.800$	0.115	0.375	0.370	0.675	0.215	0.555	0.495	0.815

outperforms general linear model (GLM), we also analyzed the simulated data using GLM, in which we fitted GLM at each  $s_m$  without separating  $\eta_{i,j}(s_m)$  from  $\epsilon_{i,j}(s_m)$ . Then, we calculated the global testing statistic except that we replaced  $\hat{\Sigma}_\eta(s_m, s_m)$  in  $S_n$  with  $\hat{\Sigma}_y(s_m, s_m)$ . Finally, we calculated the p-values with the wild bootstrap method as in FADTTS. Table 1 shows that GLM is much less powerful than FADTTS; see also Fig. 2. An advantage of using FADTTS is that it is capable of modeling the structured inter-subject variability, in addition to a standard white noise model. Therefore, although the parameter estimators calculated from the two methods are close to each other, the covariance estimate of these parameter estimators in GLM is larger than those in FADTTS. Moreover, standard GLM ignores the correlation among the data at different grid points.

We carried out the second set of Monte Carlo simulations to evaluate the coverage probabilities of the confidence bands for regression coefficients. For simplicity, we only simulated the MD measure along the right internal capsule tract (Fig. 8(c)) according to

$$MD_i(s_m) = \beta_1(s_m) + \beta_2(s_m) \times G_i + \beta_3(s_m) \times \text{Gage}_i + \eta_i(s_m) + \epsilon_i(s_m), \tag{14}$$

where  $\eta_i(s)$  is a Gaussian process with zero mean and covariance  $\sigma_\eta(s, t)$  and  $\epsilon_i(s)$  is a Gaussian random variable with zero mean and covariance  $\sigma_\epsilon(s, t)1(s=t)$ . We used the MD measure along the right internal capsule tract from all 128 infants in our clinical study to estimate  $\hat{B}(s)$  of  $B(s)$ ,  $\hat{\eta}(s)$  of  $\eta(s)$ , and  $\hat{\epsilon}(s)$  of  $\epsilon(s)$ , respectively. We fixed all the parameters at their estimated values and assumed them to be the true values. Subsequently, we generated random samples  $\tau_i$  and  $\tau_i(s_m)$  from a  $N(0, 1)$  generator for  $i = 1, \dots, n$  and  $m = 1, \dots, M$  and then constructed

$$MD_i(s_m)^{(g)} = \hat{\beta}_1(s_m) + \hat{\beta}_2(s_m) \times G_i + \hat{\beta}_3(s_m) \times \text{Gage}_i + \tau_i \hat{\eta}_i(s_m) + \tau_i(s_m) \hat{\epsilon}_i(s_m).$$

Based on the generated MD values  $MD_i(s_m)^{(g)}$  for  $i = 1, \dots, n$  and  $m = 1, \dots, M$ , we calculated the simultaneous confidence bands of functional coefficients  $\hat{\beta}_1(s)$ ,  $\hat{\beta}_2(s)$  and  $\hat{\beta}_3(s)$  for all  $s$ . The 95% and 99% simultaneous confidence bands were considered. As noted by Fan and Zhang (2000) and Ghouch and Genton (2009) among many others, an appropriate smaller bandwidth would improve the coverage probability of the confidence bands. In our simulations, we found that a shrinkage factor of 0.8 generally works well. For simplicity and computational efficiency, we do not consider estimating the bias of  $\hat{\beta}(s)$ .

Based on 1000 simulated data sets, the empirical coverage probabilities of  $\hat{\beta}_1(s)$ ,  $\hat{\beta}_2(s)$  and  $\hat{\beta}_3(s)$  for the significance level  $\alpha = 0.01$  (or  $\alpha = 0.05$ ) are, respectively, 0.991, 0.994, and 0.978 (0.948, 0.952 and 0.926). The coverage probabilities are quite close to the claimed confidence levels. Figs. 5 and 9 depict typical simultaneous confidence bands.

*A real example*

This clinical study was approved by the Institutional Review Board of the University of North Carolina at Chapel Hill. A total of 128

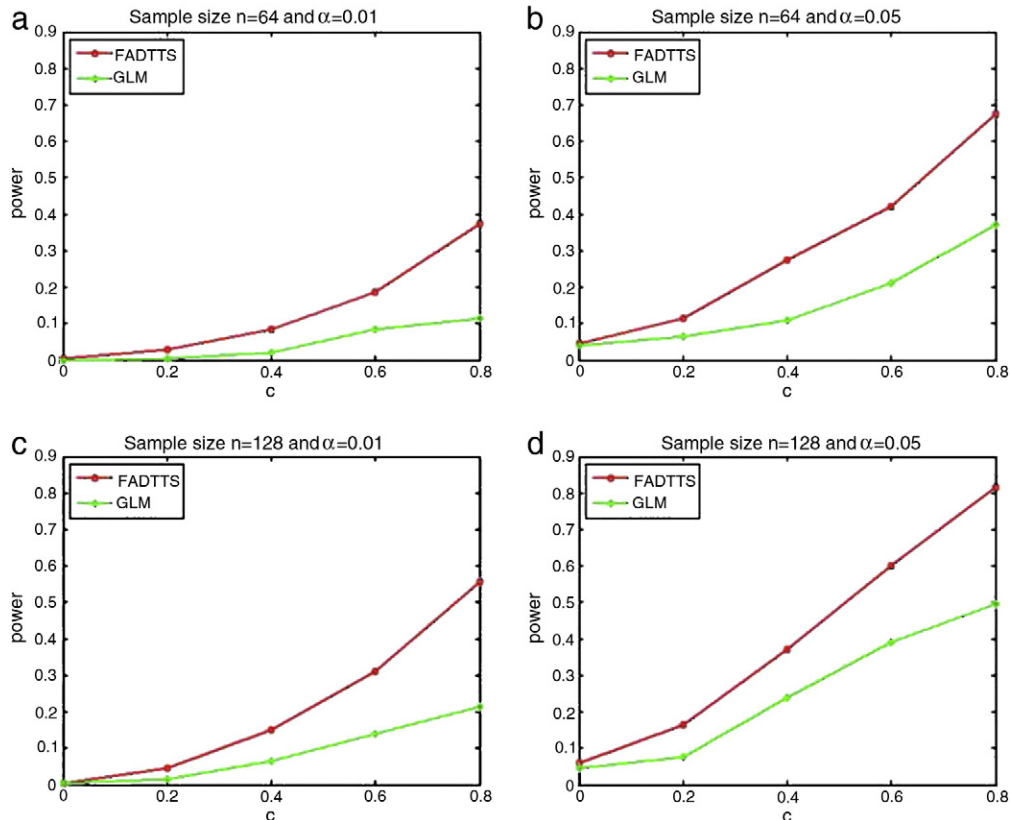


**Fig. 2.** Simulation study: Type I and Type II error rates. Rejection rates of  $S_n$  based on the resampling method are calculated at five different values of  $c$  (representing different effect sizes) for sample sizes  $n = 64$  and  $n = 128$  at  $\alpha = .05$  and  $\alpha = .01$  significance levels.

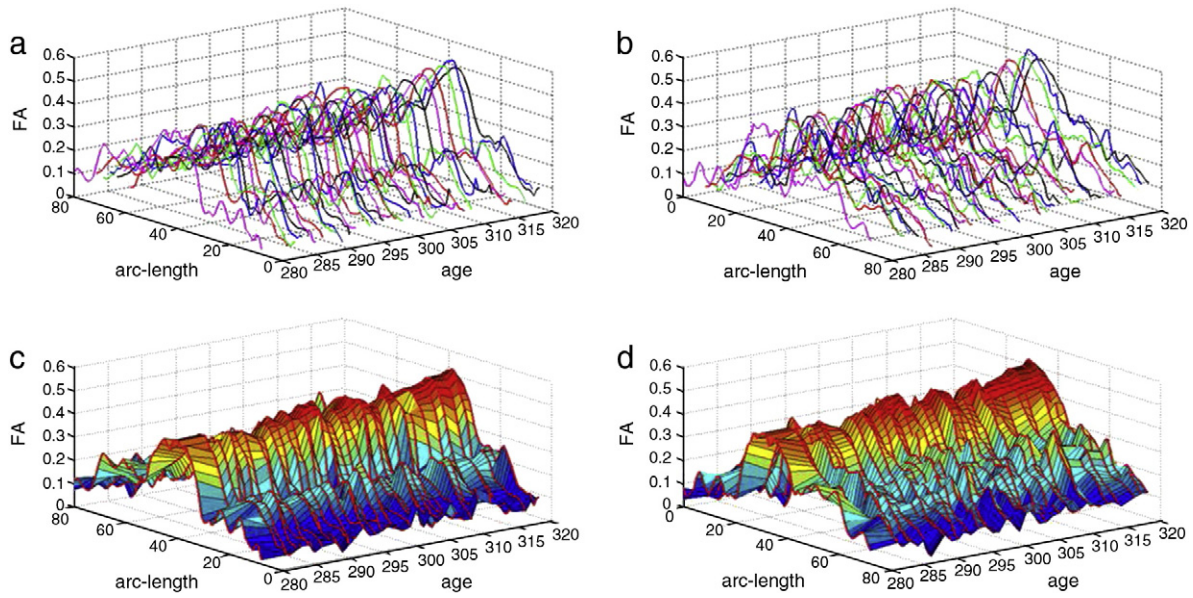


Fig. 3. 3D plots of FA along the right internal capsule tract to illustrate the possible age effect: (a) and (b) 3D line plot and (c) and (d) 3D surf plot.

healthy full-term infants (75 males and 53 females) were taken from a larger study designated to investigate early brain development. All 128 infants were less than one year old, and the written informed consent was obtained from their parents before imaging acquisition. The mean gestational age at MR scanning of the 128 infants was  $298 \pm 17.6$  days (range: 262 to 433 days). All infants were fed and calmed to

sleep on a warm blanket with proper ear protection. Technicians ensured that they slept comfortably inside the MR scanner. None of them was sedated during the imaging session.

A 3 T Allegra head-only MR system (Siemens Medical Inc., Erlangen, Germany) was used to acquire all the images. The system was equipped with a maximal gradient strength of 40 mT/m and a

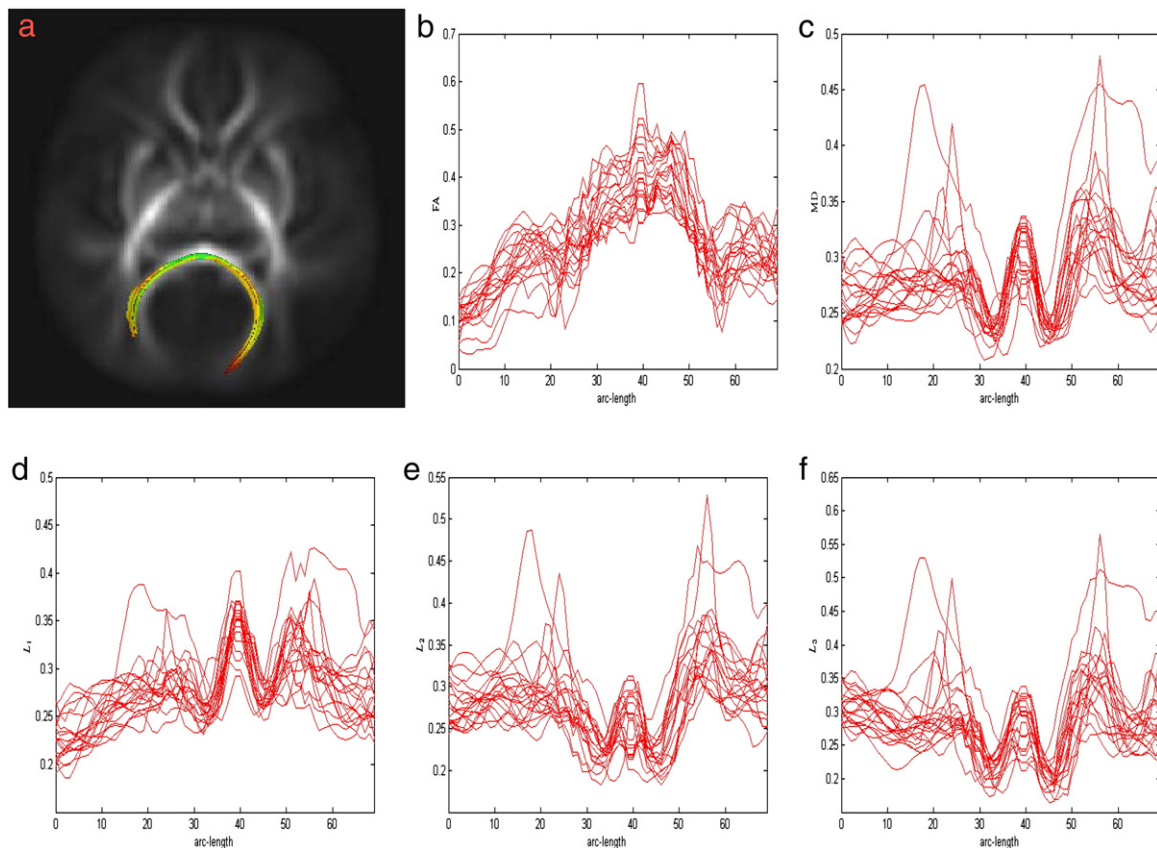
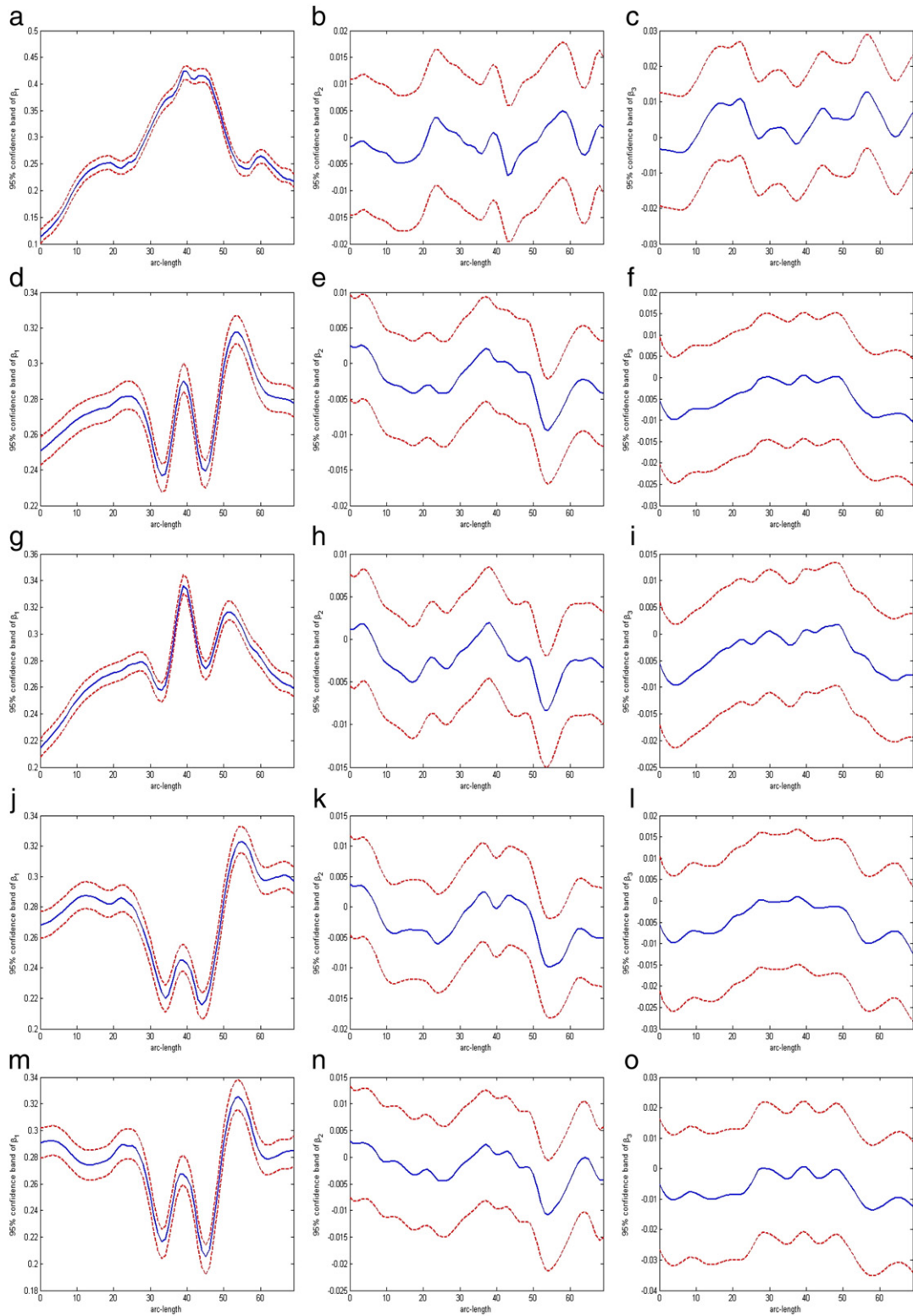


Fig. 4. Splenium tract and diffusion properties along the splenium tract: (a) the splenium tract extracted from the tensor atlas with color presenting the mean FA values; (b) FA; (c) MD; (d)  $L_1$ ; (e)  $L_2$ ; and (f)  $L_3$ . The diffusion properties in panels (b)–(f) are from 20 randomly selected infants.



**Fig. 5.** The estimated coefficient functions (blue solid lines) and the corresponding 95% confidence bands (red dashed lines) for the five measures along the splenium tract: (a), (d), (g), (j), and (m) the varying intercept functions for FA, MD,  $L_1$ ,  $L_2$  and  $L_3$ , respectively; (b), (e), (h), (k), and (n) the varying coefficient functions of gender for FA, MD,  $L_1$ ,  $L_2$  and  $L_3$ , respectively; (c), (f), (i), (l), and (o) the varying coefficient functions associated with gestational age for FA, MD,  $L_1$ ,  $L_2$  and  $L_3$ , respectively.

maximal slew rate of 400 mT/(m · ms). The DTI images were obtained by using a single shot EPI DTI sequence (TR/TE = 5400/73 ms) with eddy current compensation. We applied the six non-collinear

directions at the  $b$ -value of 1000 s/mm<sup>2</sup> with a reference scan ( $b = 0$ ). The voxel resolution was isotropic 2 mm, and the in-plane field of view was set at 256 mm in both directions. To improve the

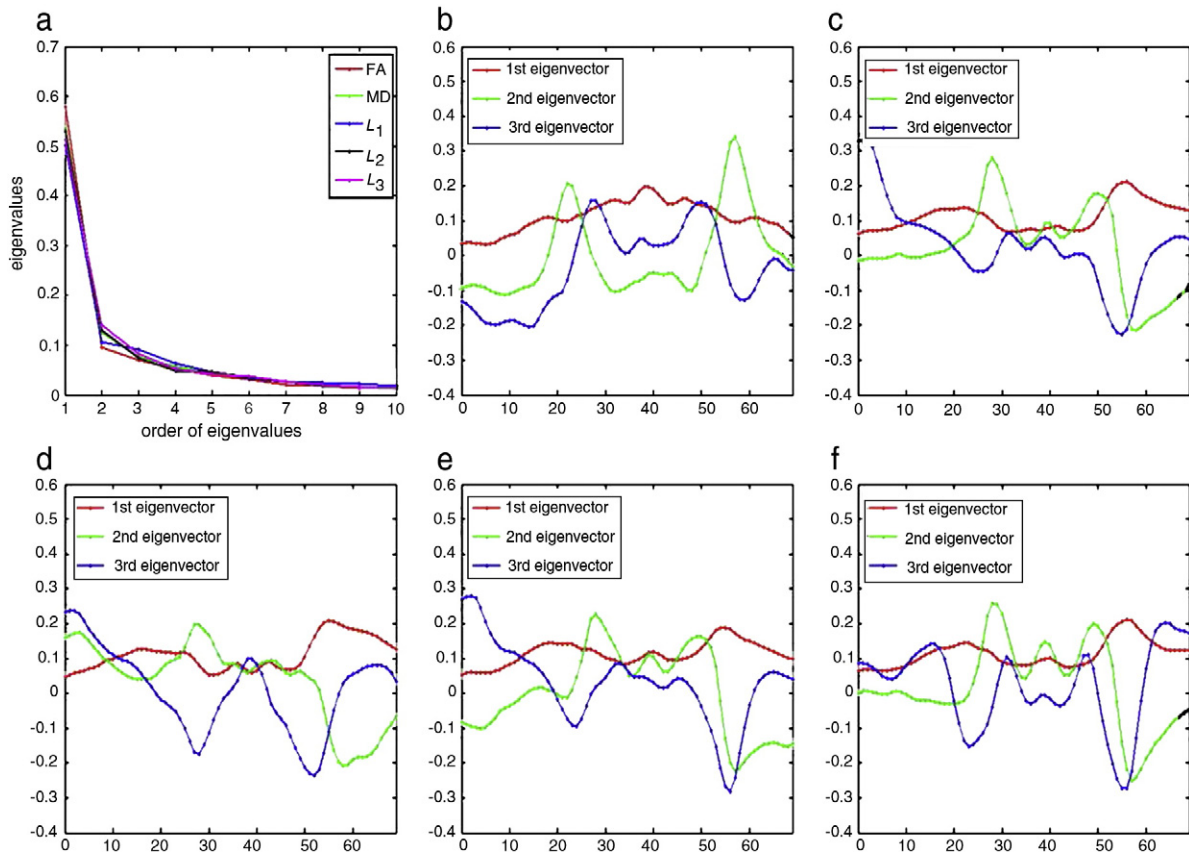


**Fig. 6.** Spectral decomposition of  $\hat{\Sigma}_{n,kk}(s, t)$  for FA, MD,  $L_1$ ,  $L_2$  and  $L_3$  along the splenium tract: (a) the first 12 relative eigenvalues; (b) the first 3 eigenvectors for FA; (c) the first 3 eigenvectors for MD; (d) the first 3 eigenvectors for  $L_1$ ; (e) the first 3 eigenvectors for  $L_2$ ; and (f) the first 3 eigenvectors for  $L_3$ .

signal-to-noise ratio of the images, a total of five scans were acquired and averaged.

To construct the diffusion tensors, we used a weighted least squares estimation method (Zhu et al., 2007b; Basser et al., 1994a). We then employed DTI atlas building followed by an atlas-based tractography procedure to process all 128 DTI datasets. While several DTI fiber tracts were tracked, we chose to focus in this paper on the splenium of the corpus callosum and the right internal capsule tract to illustrate the applicability of our method (Figs. 4 and 8). Five diffusion properties were extracted along the selected fiber tracts including FA, MD, and the three eigenvalues of the diffusion tensors, denoted by  $L_1 \geq L_2 \geq L_3$ , at each grid point along all fiber tracts of interest for all 128

infants (Goodlett et al., 2009). FA and MD, respectively, measure the inhomogeneous extent of local barriers to water diffusion and the averaged magnitude of local water diffusion, while  $L_j (j = 1, 2, 3)$  reflects the magnitude of water diffusivity along and perpendicular to the long axis of white matter fibers (Song et al., 2003).

In this study, we have two specific aims. The first is to compare diffusion properties along the selected fiber bundles across the male and female groups and thus illuminate the gender effect on the development of these fiber bundle diffusion properties. The second is to delineate the development of fiber bundle diffusion properties across time—the age effect. As a graphical illustration, we plotted FA measures along the right internal capsule tract from 40 randomly

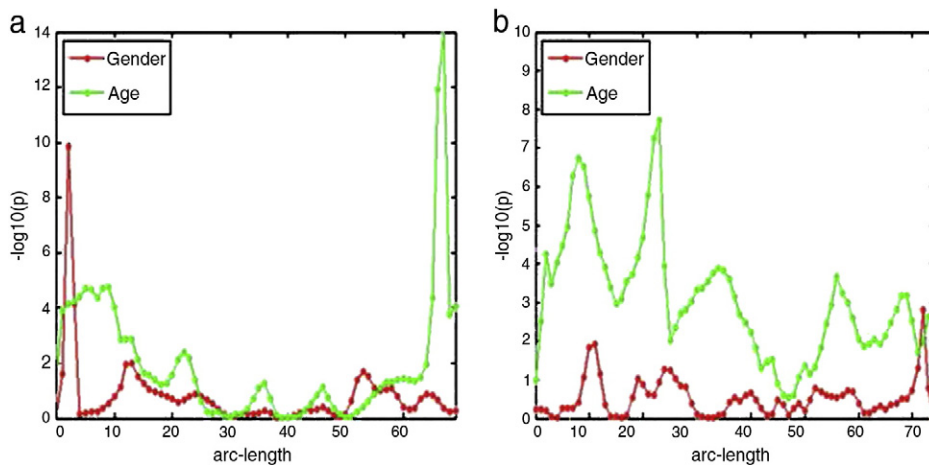


**Fig. 7.**  $-\log_{10}(p)$  values for testing gender and gestational age effects of test statistics  $S_n(s_j)$  for the two selected tracts: (a)  $-\log_{10}(p)$  values for testing gender and gestational age effects of the splenium tract; (b)  $-\log_{10}(p)$  values for testing gender and gestational age effects of the right internal capsule tract.

selected infants (Fig. 3). We observed that the values of FA increase with gestational age at nearly all grid points. To statistically test the gender and age effects, we applied our FADTTS to the joint analysis of FA and MD values and the three eigenvalues along each of the two tracts.

For the two selected tracts, we fit the multivariate varying coefficient model (1) to the smoothed FA and MD values and the three eigenvalues from all 128 subjects, in which  $\mathbf{x} = (1, G, \text{Gage})^T$  and  $M=5$ . We then estimated the functional coefficients  $B(s)$ . In the functional principal component analysis, we estimated  $\eta(s)$  and constructed the spectral decomposition of  $\hat{\Sigma}_{\eta,ij}(s, t)$  for all  $j=1, \dots, J$  by calculating their eigenvalues and eigenfunctions. For the hypothesis testing, we constructed the global test statistic  $S_n$  via Eq. (10) to test the gender and age effects for the five diffusion-tensor properties altogether. We approximated the  $p$ -value of  $S_n$  using the resampling method with  $G = 1000$  replications. Finally, we constructed the 95% simultaneous confidence bands for the functional coefficients  $B(s)$ .

The bandwidths selected by GCV for the five diffusion properties along the right internal capsule tract are, respectively, 0.49, 0.68, 0.63, 0.74 and 0.58. Fig. 5 presents the estimated varying functional coefficients  $\hat{B}(s)$  associated with all five diffusion properties (blue solid lines in all panels of Fig. 5). The intercept functions (all panels in the first column of Fig. 5) described the overall trend of the five diffusion properties. Compared with the estimated mean functions using FRATS (Zhu et al., 2010c), they produced almost identical curves, which indicates the effectiveness of FADTTS. The gender coefficients for MD and all three eigenvalues (panels (e), (h), (k), and (n) of Fig. 5) are negative at most of the grid points, which may indicate that compared with female infants, male infants have relatively smaller magnitudes of local water diffusivity along the

splenium of the corpus callosum. However, the fact that we did observe positive gender effects at some grid point may weaken our findings. We did not observe this pattern for FA (panel (b) of Fig. 5). The gestational age coefficients for FA (panel (c) of Fig. 5) are positive at most grid points, indicating that FA measures increase with age in both male and female infants, whereas those corresponding to MD and all three eigenvalues (panels (f), (i), (l), and (o) of Fig. 5) are negative at most grid points. This may indicate a negative correlation between the magnitudes of local water diffusivity and gestational age along the splenium of the corpus callosum. It also has been noted that we did observe negative age effects at some grid points of FA and positive age effects of the other four diffusion properties at some grid points, which again may weaken our findings.

We presented the eigenvalues and eigenfunctions of  $\hat{\Sigma}_{\eta,ij}(s, t)$  for all  $j=1, \dots, J$  in Fig. 6. For all five measures, the relative eigenvalues of  $\hat{\Sigma}_{\eta,ij}$  defined as the ratios of the eigenvalues of  $\hat{\Sigma}_{\eta,ij}(s, t)$  over their sum have almost identical distributional patterns (panel (a) of Fig. 6). We observed that the first three relative eigenvalues account for 80% of the total and the others quickly vanish to zero. The eigenfunctions of FA corresponding to the largest three eigenvalues (Fig. 6(b)) are different from those of the other four measures (Figs. 6(c)–(f)). For MD,  $L_1$ ,  $L_2$ , and  $L_3$ , similar patterns were observed among the eigenfunctions corresponding to the largest three eigenvalues. This is consistent with the fact that FA is a scaled-invariant measure of all the eigenvalues.

We statistically test the effects of gender and gestational age on all five diffusion properties along the splenium tract. To test the gender effect, we calculated the local test statistics  $S_n(s_m)$  and their corresponding  $p$ -values across all grid points on the splenium tract; only a few grid points have  $-\log_{10}(p)$  values greater than 2 (red line

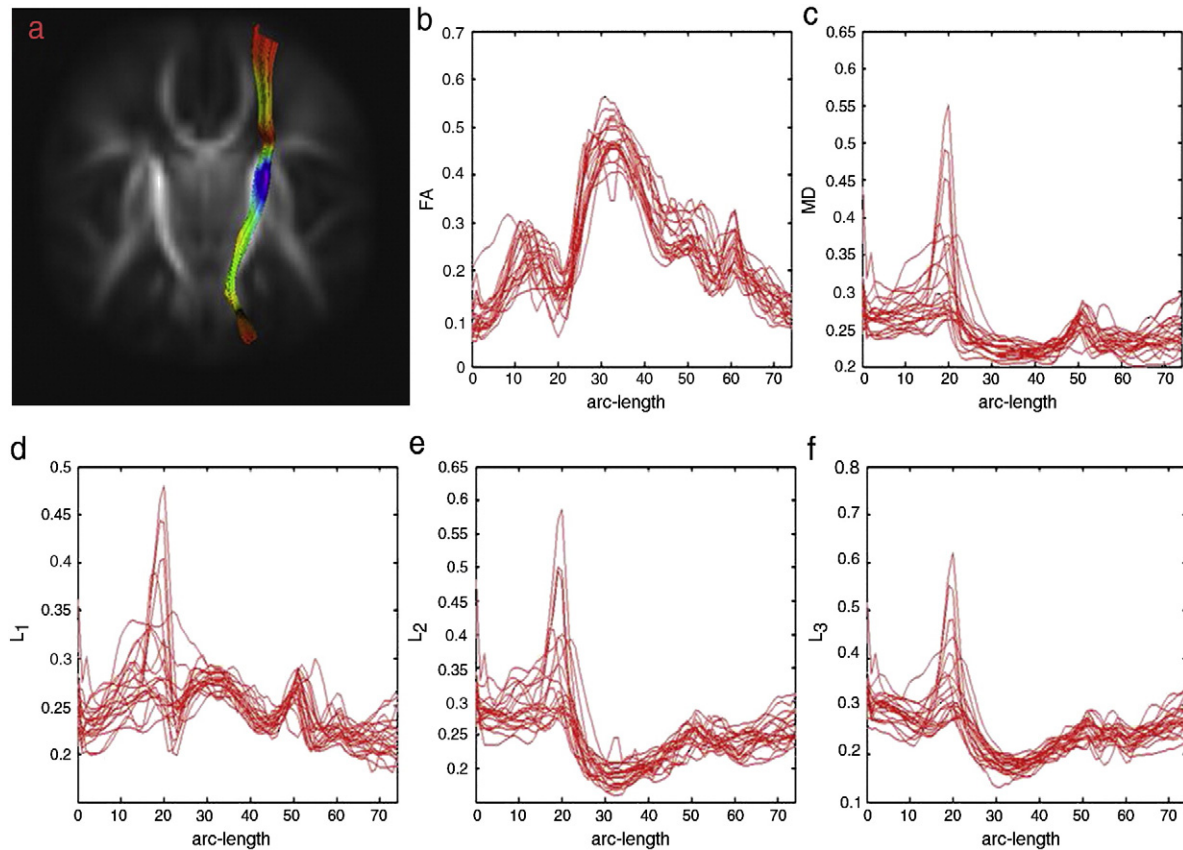
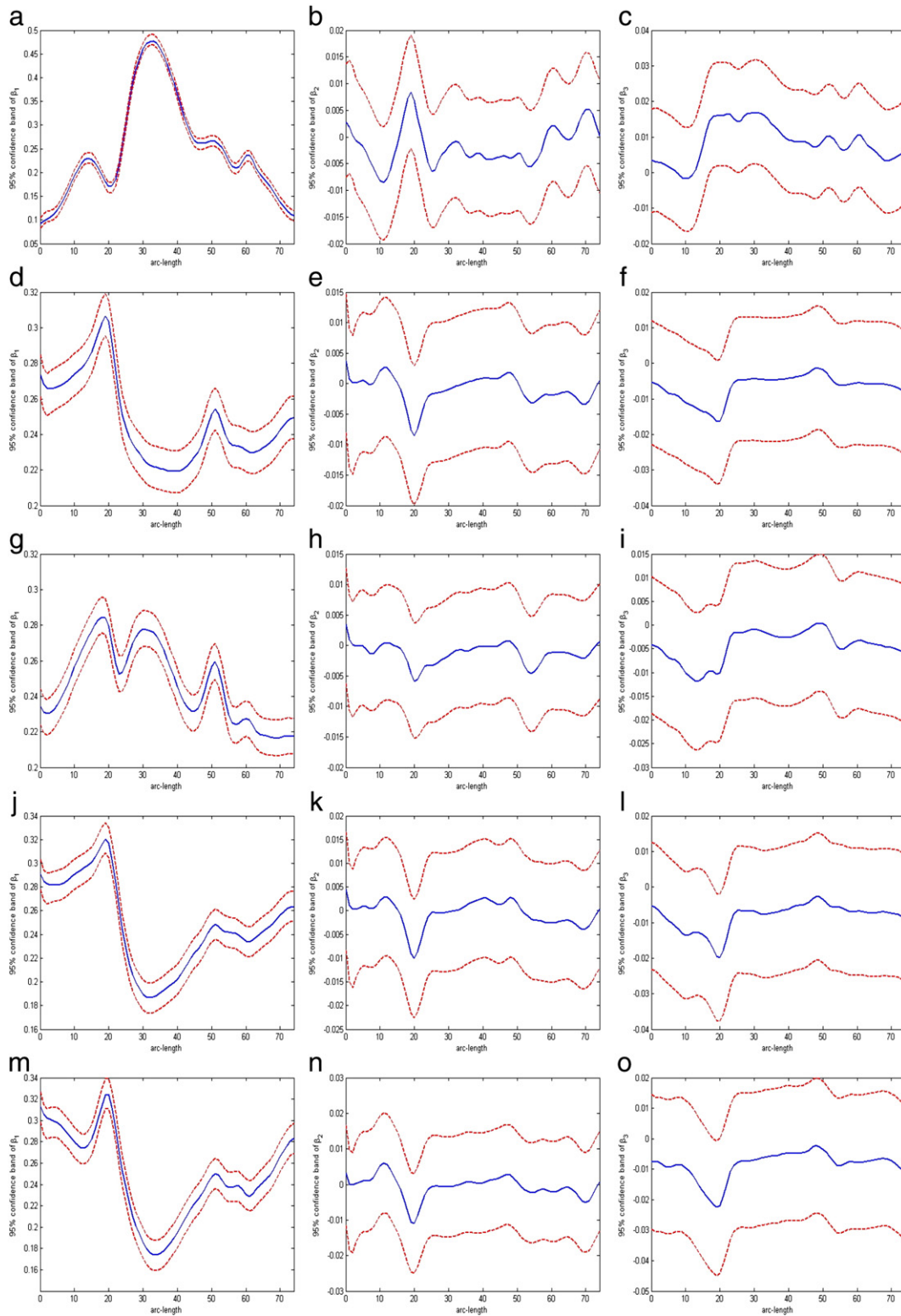


Fig. 8. Right internal capsule and diffusion properties along the right internal capsule tract: (a) the right internal capsule tract extracted from the tensor atlas with color presenting the mean FA values; (b) FA; (c) MD; (d)  $L_1$ ; (e)  $L_2$ ; and (f)  $L_3$ . The diffusion properties in panels (b)–(f) are from 20 randomly selected infants.



**Fig. 9.** The estimated coefficient functions (blue solid lines) and the corresponding 95% confidence bands (red dashed lines) for the five measures along the right internal capsule tract. Panels (a), (d), (g), (j), and (m) are the varying intercept functions for FA, MD,  $L_1$ ,  $L_2$  and  $L_3$ , respectively. Panels (b), (e), (h), (k), and (n) are the varying coefficient functions of gender for FA, MD,  $L_1$ ,  $L_2$  and  $L_3$ , respectively. Panels (c), (f), (i), (l), and (o) are the varying coefficient functions of gestational age for FA, MD,  $L_1$ ,  $L_2$  and  $L_3$ , respectively.

in Fig. 7(a)). Then, we computed the global test statistic  $S_n = 506.69$  and its associated  $p$ -value ( $p = 0.054$ ), indicating a weakly significant gender effect, which agrees with the findings in panels (e), (h), (k), and (n) of Fig. 5. The  $-\log_{10}(p)$  values of  $S_n(S_m)$  for testing the age effect at most grid points are greater than 2 (green line in Fig. 7(a)),

while a moderately significant age effect was found with  $S_n = 971.16$  ( $p$ -value = .034). This agrees with the findings in panels (c), (f), (i), (l), and (o) of Fig. 5, indicating that some diffusion properties along the splenium tract differ slightly between male and female groups and change moderately with gestational age. Furthermore, for all diffusion

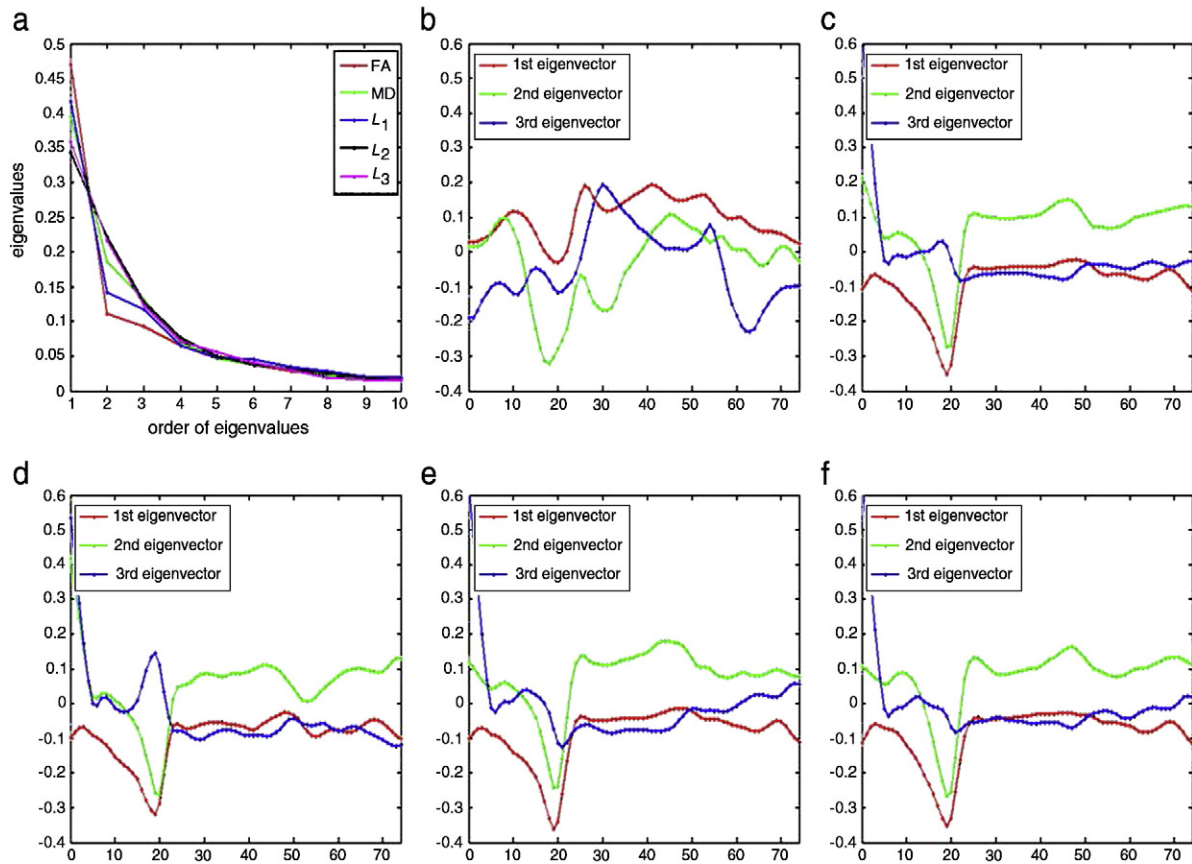


**Fig. 10.** Spectral decomposition of  $\Sigma_{\eta,kk}(s,t)$  for FA, MD,  $L_1$ ,  $L_2$  and  $L_3$  along the right internal capsule tract: (a) the first 12 relative eigenvalues for FA, MD,  $L_1$ ,  $L_2$  and  $L_3$ ; (b) the first 3 eigenvectors for FA; (c) the first 3 eigenvectors for MD; (d) the first 3 eigenvectors for  $L_1$ ; (e) the first 3 eigenvectors for  $L_2$ ; and (f) the first 3 eigenvectors for  $L_3$ .

properties, we constructed the 95% simultaneous confidence bands of the varying coefficients for  $G_i$  and  $Gage_i$  (Fig. 5).

For the right internal capsule tract, we have the following findings. Fig. 9 presents the estimated  $\hat{B}(s)$  associated with all diffusion properties along the right internal capsule tract (blue solid lines in all panels of Fig. 9). Since the patterns in Fig. 9 were similar to those in Fig. 5, we do not repeat them here. Moreover, for  $j = 1, \dots, 5$ , Fig. 10 presents the relative eigenvalues and eigenvectors of  $\hat{\Sigma}_{\eta,ij}(s,t)$  along the right internal capsule tract. As shown in Fig. 10(a), the first three relative eigenvalues account for the 70% of the total, and the rest quickly vanish to zero. For all diffusion properties, the eigenfunctions associated with the largest first eigenvalues for the right capsule tract (panels (b)–(f) of Fig. 10) show patterns similar to those for the splenium tract in Fig. 6. Moreover, we found no significant effect of gender since  $S_n = 420.05$  with a  $p$ -value of 0.347, even though the  $-\log_{10}(p)$  values of  $S_n(s_m)$  for gender are greater than 2 at a few grid points (red line in Fig. 7(b)). However, a highly significant effect of gestational age was found with  $S_n = 1549.1$  and its  $p$ -value  $p < 0.001$ ,

while the  $-\log_{10}(p)$  values of  $S_n(s_m)$  for the age effect are greater than 2 at all grid points (green line in Fig. 7(b)). This indicates that diffusion properties along the right internal capsule tract do not differ significantly between male and female groups but are significantly associated with gestational age. Finally, we constructed 95% simultaneous confidence bands for the functional coefficients (Fig. 9).

In our last step, we applied FADTTS to each of the five diffusion properties along both the right internal capsule tract and the splenium tract and then calculated the global test statistic  $S_n$  and its associated  $p$ -value (Table 2). For the splenium tract, recall the overall  $p$ -values  $p = 0.054$  and  $p = 0.034$  for the gender effect and the age effect, respectively, based on all five diffusion properties. Inspecting individual diffusion properties reveals that gender mainly has a mild effect on MD,  $L_1$  and  $L_2$ , while age influences MD and the three eigenvalues. These results agree with the findings in Fig. 9. For the right internal capsule tract, the overall  $p$ -values are given by  $p = 0.347$  and  $p < 0.001$  for the gender effect and the age effect, respectively, based on all five diffusion properties. We did not observe a gender effect on any of the five individual diffusion properties, but there are significant age effects on all of them.

**Table 2**  
The  $p$ -values of  $S_n$  for testing the effects of gender and gestational age on the splenium and right internal capsule tracts.

	Splenium		Right internal capsule	
	Gender	Gestational age	Gender	Gestational age
FA	0.683	0.103	0.169	<0.001
MD	0.063	0.008	0.354	<0.001
$L_1$	0.048	0.003	0.241	<0.001
$L_2$	0.057	0.007	0.314	<0.001
$L_3$	0.302	0.010	0.376	<0.001
(FA, MD, $L_1$ , $L_2$ , $L_3$ )	0.054	0.034	0.347	<0.001

**Discussion**

The contributions of our work are twofold. From the statistical perspective, we have developed a new functional analysis pipeline for delineating the structure of the variability of multiple diffusion properties along major white matter fiber bundles and their association with a set of covariates of interest. The FADTTS pipeline integrates five advanced statistical tools from the statistical literature. From the application perspective, we have demonstrated FADTTS in a clinical study of neurodevelopment for revealing the complex

inhomogeneous spatiotemporal maturation patterns as the apparent changes in fiber bundle diffusion properties. We expect that this novel statistical tool will lead to new findings in our clinical applications.

Several limitations need to be addressed in future research. Even though the three eigenvalues satisfy the constraint  $L_1 \geq L_2 \geq L_3$ , model (1) and its associated statistical procedure do not impose such a constraint. Moreover, for some strongly nondegenerate tensors ( $L_1 > L_2 > L_3$ ) with small  $L_2$  and  $L_3$ , there may be difficulty in distinguishing these two smallest eigenvalues. It is also possible that the fitted mean eigenvalues obtained from model (1) may be negative. A possible solution is to require that the fitted eigenvalue in model (1) be non-negative; an alternative solution is to use the logarithm of eigenvalues as responses. Both are topics for future research.

All fiber tract based methods including FADTTS are only applicable to these major white matter tracts in which one can establish the common localization across subjects. Thus, FADTTS is able to investigate a subset of different scenarios in which white matter structure is associated with a covariate, such as age, gender, and diagnostic status. For instance, the centroid of the localization of white matter lesion could vary across time and subjects. In this case, neither ROI based methods nor tract based methods would be appropriate. In some heterogenous populations, it is possible that tract-specific changes occur in only a subset of subjects.

There are several current topics for our research. We are developing new statistical methods for making statistical inferences about both the eigenvalues and eigenfunctions in FPCA and for establishing the association of eigenvalues and eigenfunctions with a set of covariates of interest. We are exploring other nonparametric methods, such as wavelet and B-spline methods instead of using local polynomial kernel. We are in the process of extending FADTTS to the analysis of high angular resolution diffusion image (HARDI), which is important for resolving the issue of fiber crossing (Lenglet et al., 2009; Tuch et al., 2002). It is also important to extend FADTTS to principal directions and full diffusion tensors on fiber bundles (Schwartzman, 2006; Lepore et al., 2008; Schwartzman et al., 2005; Zhu et al., 2009; Whitcher et al., 2007). The proposed methodology can be readily extended to more complex fiber structures, such as the medial manifolds of fiber tracts (Yushkevich et al., 2008). Furthermore, we will extend FADTTS to longitudinal studies and family studies (Fang and Wang, 2009). Finally, we have treated fiber bundle diffusion properties as functional responses. It will be interesting to consider generalized functional linear models, in which a scalar outcome (e.g., diagnostic group) is used as the response and fiber bundle diffusion properties are used as varying covariate functions (or functional predictor) (Ramsay and Silverman, 2005; Goldsmith et al., in press).

## Appendix A. Supplementary data

Supplementary data to this article can be found online at doi:10.1016/j.neuroimage.2011.01.075.

## References

- Ashburner, J., Friston, K.J., 2000. Voxel-based morphometry: the methods. *Neuroimage* 11, 805–821.
- Basser, P.J., Mattiello, J., LeBihan, D., 1994a. Estimation of the effective self-diffusion tensor from the NMR spin echo. *J. Magn. Reson. B* 103, 247–254.
- Basser, P.J., Mattiello, J., LeBihan, D., 1994b. MR diffusion tensor spectroscopy and imaging. *Biophys. J.* 66, 259–267.
- Bonekam, D., Nagae, L.M., Degaonkar, M., Matson, M., Abdalla, W.M., Barker, P.B., Mori, S., Horska, A., 2008. Diffusion tensor imaging in children and adolescents: reproducibility, hemispheric, and age-related differences. *Neuroimage* 34, 733–742.
- Camara, E., Bodammer, N., Rodriguez-Fornells, A., Tempelmann, C., 2007. Age-related water diffusion changes in human brain: a voxel-based approach. *Neuroimage* 34, 1588–1599.
- Cascio, C.J., Gerig, G., Piven, J., 2007. Diffusion tensor imaging: application to the study of the developing brain. *J. Am. Acad. Child Adolesc. Psychiatry* 46, 213–223.
- Chen, Y.S., An, H.Y., Zhu, H.T., Stone, T., Smith, J.K., Hall, C., Bullitt, E., Shen, D.G., Lin, W.L., 2009. White matter abnormalities revealed by diffusion tensor imaging in non-demented and demented HIV+ patients. *Neuroimage* 47, 1154–1162.
- Fan, J., Gijbels, I., 1996. *Local Polynomial Modelling and Its Applications*. Chapman and Hall, London.
- Fan, J., Zhang, W., 1999. Statistical estimation in varying coefficient models. *Ann. Stat.* 27 (5), 1491–1518.
- Fan, J., Zhang, W., 2000. Simultaneous confidence bands and hypothesis testing in varying-coefficient models. *Scand. J. Stat.* 27 (4), 715–731.
- Fan, J., Zhang, W., 2008. Statistical methods with varying coefficient models. *Stat. Interface* 1 (1), 179–195.
- Fan, J., Yao, Q., Cai, Z., 2003. Adaptive varying-coefficient linear models. *J. R. Stat. Soc. B Stat. Methodol.* 65 (1), 57–80.
- Fang, Y., Wang, Y., 2009. Testing for familial aggregation of functional traits. *Stat. Med.* 28, 3611–3625.
- Ferguson, C.A., Bowman, A.W., Scott, E.M., Carvalho, L., 2009. Multivariate varying-coefficient models for an ecological system. *Environmetrics* 20, 460–476.
- Focke, N.K., Yogarajah, M., Bonelli, S.B., Bartlett, P.A., Symms, M.R., Duncan, J.S., 2008. Voxel-based diffusion tensor imaging in patients with mesial temporal lobe epilepsy and hippocampal sclerosis. *Neuroimage* 40, 728–737.
- Ghouch, A.E., Genton, M.G., 2009. Local polynomial quantile regression with parametric features. *J. Am. Stat. Assoc.* 104, 1416–1429.
- Gilmore, J.H., Smith, L.C., Wolfe, H.M., Hertzberg, B.S., Smith, J.K., Chescheir, N.C., Evans, D.D., Kang, C., Hamer, R.M., Lin, W., Gerig, G., 2008. Prenatal mild ventriculomegaly predicts abnormal development of the neonatal brain. *Biol. Psychiatry* 64, 1069–1076.
- Goldsmith, A., Feder, J., Crainiceanu, C., Caffo, B., Reich, D., in press. Penalized functional regression. *J. Comput. Graph. Stat.*
- Goodlett, C.B., Fletcher, P.T., Gilmore, J.H., Gerig, G., 2009. Group analysis of DTI fiber tract statistics with application to neurodevelopment. *Neuroimage* 45, S133–S142.
- Gouttard, S., Prastawa, M., Bullitt, E., Lin, W., Goodlett, C., Gerig, G., 2009. Constrained data decomposition and regression for analyzing healthy aging from fiber tract diffusion properties. In: Yang, G.-Z., Hawkes, D., Rueckert, D., Noble, A., Taylor, C. (Eds.), *Medical Image Computing and Computer-Assisted Intervention – MICCAI 2009*, Volume 5761 of Lecture Notes in Computer Science. Springer Berlin/Heidelberg, pp. 321–328.
- Greven, S., Crainiceanu, C., Caffo, B., Reich, D., 2010. Longitudinal functional principal component analysis. *Electron. J. Stat.* 4, 1022–1054.
- Hall, P., Müller, H.-G., Wang, J.-L., 2006. Properties of principal component methods for functional and longitudinal data analysis. *Ann. Stat.* 34 (3), 1493–1517.
- Hasan, K.M., Narayana, P.A., 2003. Computation of the fractional anisotropy and mean diffusivity maps without tensor decoding and diagonalization: theoretical analysis and validation. *Magn. Reson. Med.* 50, 589–598.
- Hasan, K.M., Basser, P.J., Parker, D.L., Alexander, A.L., 2001. Analytical computation of the eigenvalues and eigenvectors in DT-MRI. *J. Magn. Reson.* 152, 41–47.
- Hecke, W.V., Sijbers, J., Backer, S.D., Poot, D., Parizel, P.M., Leemans, A., 2009. On the construction of a ground truth framework for evaluating voxel-based diffusion tensor MRI analysis methods. *Neuroimage* 46, 692–707.
- Jones, D.K., Symms, M.R., Cercignani, M., Howard, R.J., 2005. The effect of filter size on VBM analyses of DT-MRI data. *Neuroimage* 26, 546–554.
- Kosorok, M.R., 2003. Bootstraps of sums of independent but not identically distributed stochastic processes. *J. Multivariate Anal.* 84, 299–318.
- Lenglet, C., Campbell, J.S.W., Descoteaux, M., Haro, G., Savadjiev, P., Wassermann, D., Anwender, A., Deriche, R., Pike, G.B., Sapiro, G., Siddiqi, K., Thompson, P.M., 2009. Mathematical methods for diffusion MRI processing. *Neuroimage* 45, S111–S122.
- Lepore, N., Brun, C.A., Chou, Y., Chiang, M., Dutton, R.A., Hayashi, K.M., Luders, E., Lopez, O.L., Aizenstein, H.J., Toga, A.W., Becker, J.T., Thompson, P.M., 2008. Generalized tensor-based morphometry of HIV/AIDS using multivariate statistics on deformation tensors. *IEEE Trans. Med. Imaging* 27, 129–141.
- Li, Y., Hsing, T., 2010. Uniform convergence rates for nonparametric regression and principal component analysis in functional/longitudinal data. *Ann. Stat.* 38, 3321–3351.
- Moseley, M., 2002. Diffusion tensor imaging and aging—a review. *NMR Biomed.* 15, 553–560.
- Mukherjee, P., McKinstry, R.C., 2006. Diffusion tensor imaging and tractography of human brain development. *Neuroimaging Clin. N. Am.* 16, 19–43.
- O'Donnell, L., Westin, C.-F., Golby, A., 2009. Tract-based morphometry for white matter group analysis. *Neuroimage* 45, 832–844.
- Pierpaoli, C., Basser, P.J., 1996. Toward a quantitative assessment of diffusion anisotropy. *Magn. Reson. Med.* 36, 893–906.
- Ramsay, J.O., Silverman, B.W., 2002. *Applied functional data analysis*. Springer Series in Statistics. Springer-Verlag, New York. Methods and case studies.
- Ramsay, J.O., Silverman, B.W., 2005. *Functional Data Analysis*. Springer-Verlag, New York.
- Rollins, N.K., 2007. Clinical applications of diffusion tensor imaging and tractography in children. *Pediatr. Radiol.* 37, 769–780.
- Schwartzman, A., 2006. *Random ellipsoids and false discovery rates: statistics for diffusion tensor imaging data*. Ph.D. thesis, Stanford University.
- Schwartzman, A., Dougherty, R.F., Taylor, J.E., 2005. Cross-subject comparison of principal diffusion direction maps. *Magn. Reson. Med.* 53, 1423–1431.
- Smith, S.M., Jenkinson, M., Johansen-Berg, H., Rueckert, D., Nichols, T.E., Mackay, C.E., Watkins, K.E., Ciccarelli, O., Cader, M., Matthews, P., Behrens, T.E., 2006. Tract-based spatial statistics: voxelwise analysis of multi-subject diffusion data. *Neuroimage* 31, 1487–1505.
- Snook, L., Paulson, L.A., Roy, D., Phillips, L., Beaulieu, C., 2005. Diffusion tensor imaging of neurodevelopment in children and young adults. *Neuroimage* 26, 1164–1173.

- Snook, L., Plewes, C., Beaulieu, C., 2007. Voxel based versus region of interest analysis in diffusion tensor imaging of neurodevelopment. *Neuroimage* 34, 243–252.
- Song, S.K., Sun, S.W., Ju, W.K., Lin, S.J., Cross, A.H., Neufeld, A.H., 2003. Diffusion tensor imaging detects and differentiates axon and myelin degeneration in mouse optic nerve after retinal ischemia. *Neuroimage* 20, 1714–1722.
- Tuch, D.S., Reese, T.G., Wiegell, M.R., Makris, N., Belliveau, J.W., Wedeen, V.J., 2002. High angular resolution diffusion imaging reveals intravoxel white matter fiber heterogeneity. *Magn. Reson. Med.* 48, 577–582.
- Wager, T.D., Keller, M., Lacey, S.C., Jonides, J., 2005. Increased sensitivity in neuroimaging analyses using robust regression. *Neuroimage* 26, 99–113.
- Wand, M.P., Jones, M.C., 1995. *Kernel Smoothing*. Chapman and Hall, London.
- Wang, L., Li, H., Huang, J.Z., 2008. Variable selection in nonparametric varying-coefficient models for analysis of repeated measurements. *J. Am. Stat. Assoc.* 103 (484), 1556–1569.
- Welsh, A.H., Yee, T.W., 2006. Local regression for vector responses. *J. Stat. Plan. Infer.* 136, 3007–3031.
- Whitcher, B., Wisco, J.J., Hadjikhani, N., Tuch, D.S., 2007. Statistical group comparison of diffusion tensors via multivariate hypothesis testing. *Magn. Reson. Med.* 57, 1065–1074.
- Worsley, K.J., Taylor, J.E., Tomaiuolo, F., Lerch, J., 2004. Unified univariate and multivariate random field theory. *Neuroimage* 23, 189–195.
- Wu, C.O., Chiang, C.-T., 2000. Kernel smoothing on varying coefficient models with longitudinal dependent variable. *Stat. Sinica* 10 (2), 433–456.
- Wu, H.L., Zhang, J.T., 2006. *Nonparametric Regression Methods for Longitudinal Data Analysis*. John Wiley & Sons, Inc., Hoboken, New Jersey.
- Yao, F., Lee, T.C.M., 2006. Penalized spline models for functional principal component analysis. *J. R. Stat. Soc. B Stat. Methodol.* 68 (1), 3–25.
- Yushkevich, P.A., Zhang, H., Simon, T., Gee, J.C., 2008. Structure-specific statistical mapping of white matter tracts. *Neuroimage* 41, 448–461.
- Zellner, A., 1962. An efficient method of estimating seemingly unrelated regressions and tests for aggregation bias. *J. Am. Stat. Assoc.* 57, 348–368.
- Zhang, J., Chen, J., 2007. Statistical inference for functional data. *Ann. Stat.* 35, 1052–1079.
- Zhu, H.T., Xu, D., Amir, R., Hao, X., Zhang, H., Alayar, K., Ravi, B., Peterson, B., 2006. A statistical framework for the classification of tensor morphologies in diffusion tensor images. *Magn. Reson. Imaging* 24, 569–582.
- Zhu, H.T., Ibrahim, J.G., Tang, N., Rowe, D., Hao, X., Bansal, R., Peterson, B.S., 2007a. A statistical analysis of brain morphology using wild bootstrapping. *IEEE Trans. Med. Imaging* 26, 954–966.
- Zhu, H.T., Zhang, H.P., Ibrahim, J.G., Peterson, B.G., 2007b. Statistical analysis of diffusion tensors in diffusion-weighted magnetic resonance image data (with discussion). *J. Am. Stat. Assoc.* 102, 1085–1102.
- Zhu, H.T., Cheng, Y.S., Ibrahim, J.G., Li, Y.M., Hall, C., Lin, W.L., 2009. Intrinsic regression models for positive definite matrices with applications in diffusion tensor images. *J. Am. Stat. Assoc.* 104, 1203–1212.
- Zhu, H., Styner, M., Li, Y., Kong, L., Shi, Y., Lin, W., Coe, C., Gilmore, J., 2010a. Multivariate varying coefficient models for DTI tract statistics. In: Jiang, T., Navab, N., Pluim, J., Viergever, M. (Eds.), *Medical Image Computing and Computer-Assisted Intervention – MICCAI 2010*, Volume 6361 of Lecture Notes in Computer Science. Springer Berlin / Heidelberg, pp. 690–697.
- Zhu, H.T., Li, R.Z., Kong, L.L., 2010b. Multivariate Varying Coefficient Models for Functional Responses. Technical report. University of North Carolina, Chapel Hill.
- Zhu, H.T., Styner, M., Tang, N.S., Liu, Z.X., Lin, W.L., Gilmore, J., 2010c. Frats: functional regression analysis of DTI tract statistics. *IEEE Trans. Med. Imaging* 29, 1039–1049.